0.1 Full-core

In this section, we compared the results from Serpent and Moltres for a full-core simulation. The first step in the calculation was to obtain the group constants using Serpent. Figure 1 displays the *xy*-plane of the model. The model includes the bottom and top reflectors. Tables **??**, **??** and **??** specify the model input parameters. To simplify Serpent's model, all the fuel columns were standard fuel columns. Additionally, the model does not include the fuel handling holes nor the coolant channels in the bottom and top reflectors. The model considered a fresh core. Based on the previous analysis, we chose the energy group structure 15*d* in Table **??**. The material temperatures were 600K and 1200K, cases that represent the Cold Zero Power (CZP) and the Hot Full Power (HFP) core states. Serpent ran 8×10^5 neutrons/cycle, 500 active cycles, and 100 inactive cycles for the calculations.

For the Moltres input file, we made the geometry and mesh using Gmsh. Taking advantage of the symmetry of the problem, the model included only a one-sixth of the full-core. The mesh had 300720 elements and 160035 nodes. The diffusion calculations had 160035 degrees of freedom (DoFs)/energy-group, and a total of 2400525 DoFs. The Moltres input files set an eigenvalue and a flux convergence tolerance of 1×10^{-8}.

Between Serpent and Moltres, we compared the multiplication factor (K_{eff}), the power distribution, and the flux shape and magnitude in different zones of the reactor. Table 1 exhibits the K_{eff} from Serpent and Moltres. Moltres values are larger than Serpent's. The values are within a 300 pcm difference.

Figures 2 and 3 show Serpent and Moltres radial power distributions. The following analysis applies for both temperatures. The first thing to came to our attention is the symmetry of the power distribution. The results are symmetric with respect to a 60° line. This result suggests that we could reduce the mesh size by a half by considering only a one-twelfth of the reactor. The next observation is that Moltres exhibits a higher power density than Serpent in the inner ring and outer rings. The power density in the middle ring is lower for Moltres case. The largest difference is in the inner ring. Overall, the results differ in less than 0.30 MW.

To compare the fluxes, we placed an axial and a radial flux detectors in arbitrary regions of the reactor. Figure 4 shows the location of the detectors. Note that the flux in Serpent is an average over the volume, while the flux in Moltres is the point-wise flux over a line. The Serpent axial detector's volume was the fuel column's volume. The Moltres axial detector's location was the center of the fuel column. The Serpent radial detector's volume had a 2°-angle and a fuel assembly's height. Both Serpent and Moltres radial detector's location was the middle of the active core's height. Moltres ran the calculations for 15 energy groups, and collapsed the results to three groups to facilitate the visualization of the results. Figures 5 and 6 show the axial and radial fluxes at 600K. In Figure 5, the fast and epithermal fluxes in Moltres are larger while the thermal flux is smaller. The flux shapes very close. The epithermal and thermal fluxes are closer in magnitude in the active core in Serpent's simulation. In Figure 6, Serpent fluxes present some 'noise'. A higher number of generations/cycle in Serpent simulations would solve it. Another alternative is using a detector with a larger volume. Additionally, the flux in Serpent shows the location of the LBPs in the fuel assemblies. A diffusion solver fails to capture such localized effects as the group constants are homogeneous in the fuel assembly. Regarding the magnitude, the fast flux in Moltres is larger while the epithermal and thermal fluxes have almost the same magnitudes. Figures 7 and 8 display the fluxes at 1200K. These results are different from the 600K case. However, we observe the same behavior for both axial and radial fluxes.

Table 1: Serpent and Moltres eigenvalues.

	Serpent	Moltres	$\Delta\rho$ [pcm]
600K	1.10869	1.11150	228
1200K	1.06138	1.06468	292

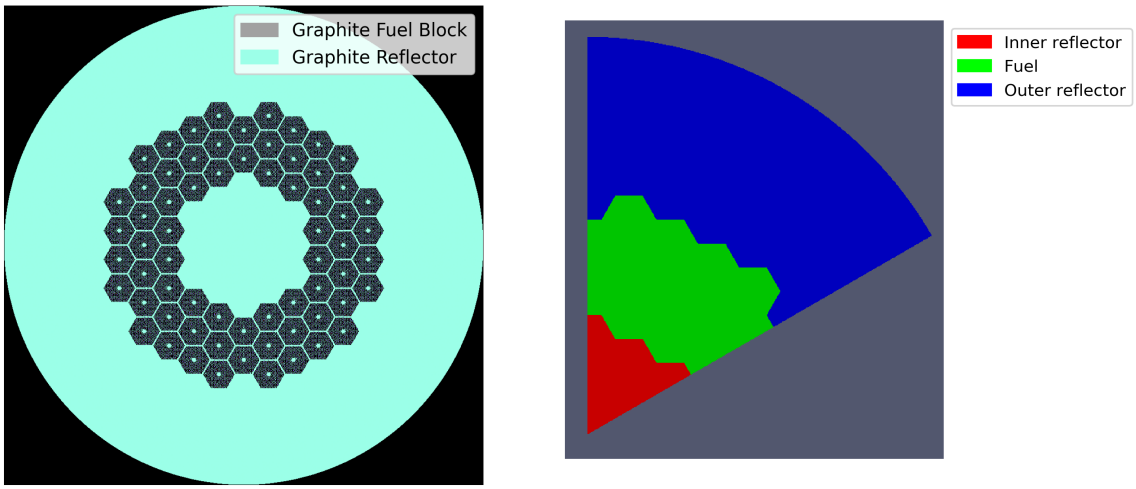

(a) Serpent model geometry.

(b) Moltres model geometry.

Figure 1: MHTGR-350 full-core models.

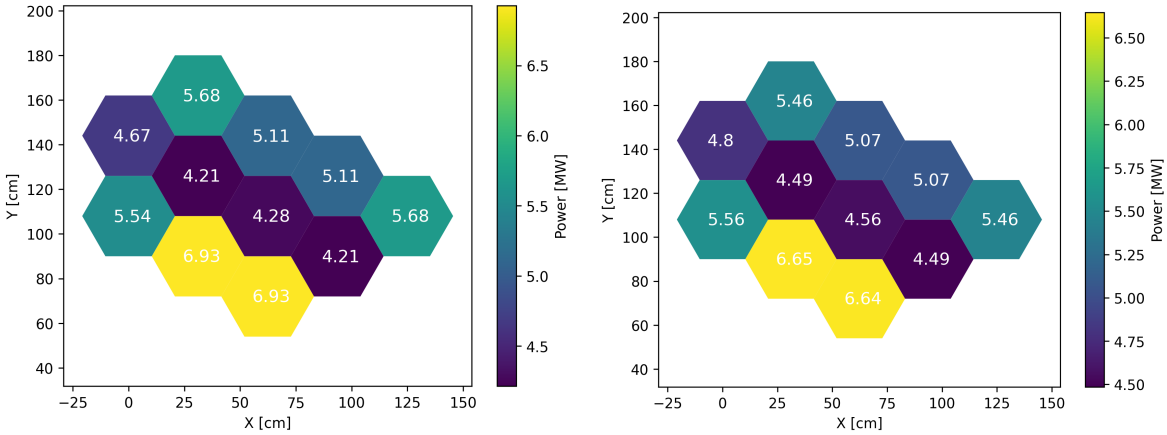

(a) Moltres.

(b) Serpent.

Figure 2: Radial power distribution at 600 K.

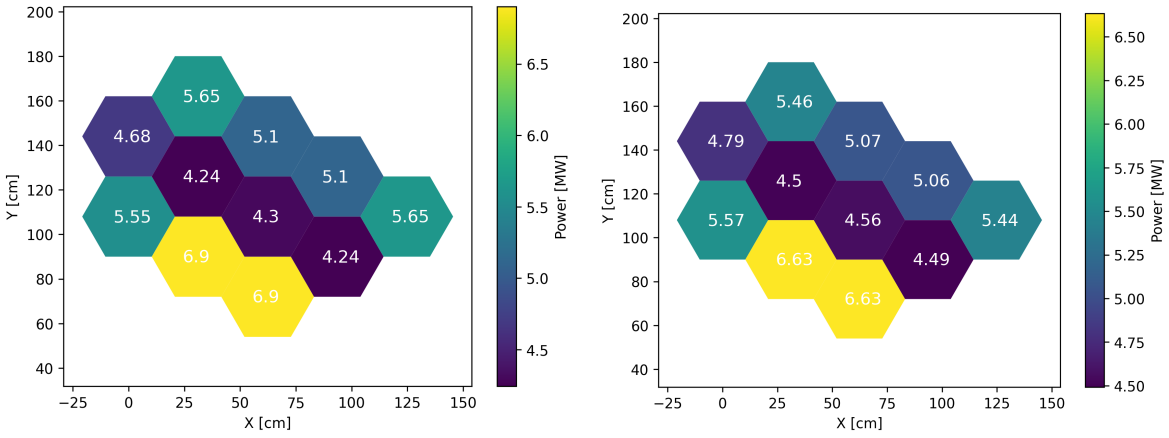

(a) Moltres. (b) Serpent.

Figure 3: Radial power distribution at 1200 K.

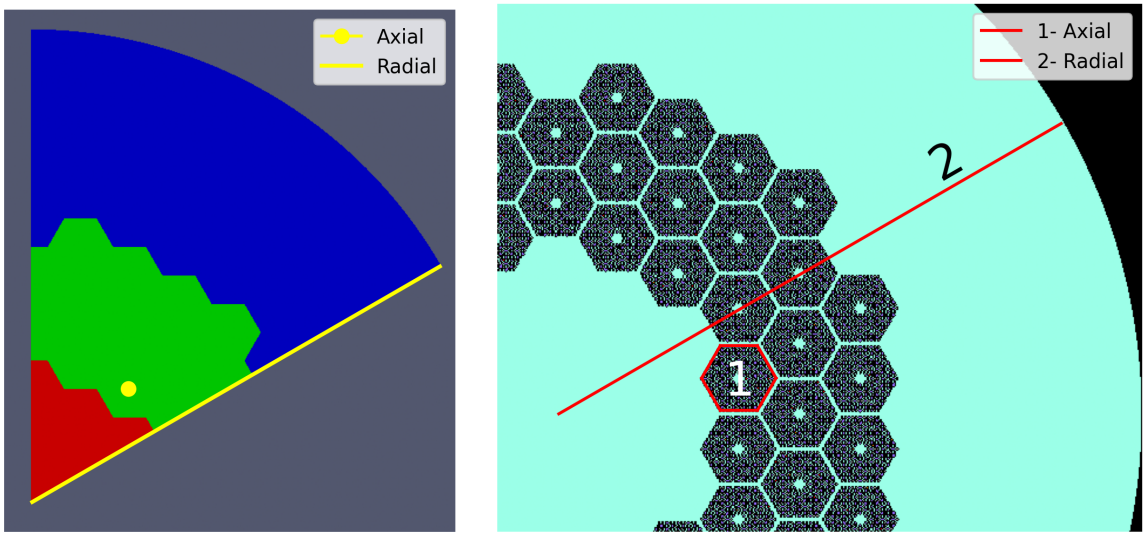

(a) (b) Serpent model geometry.

Figure 4: Flux detector locations.

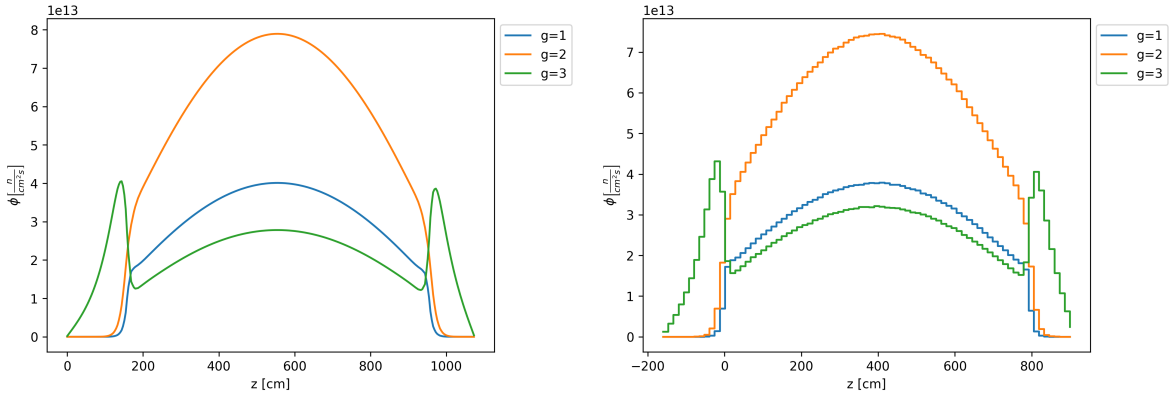

(a) (b) Serpent model geometry.

Figure 5: Axial flux at 600 K.

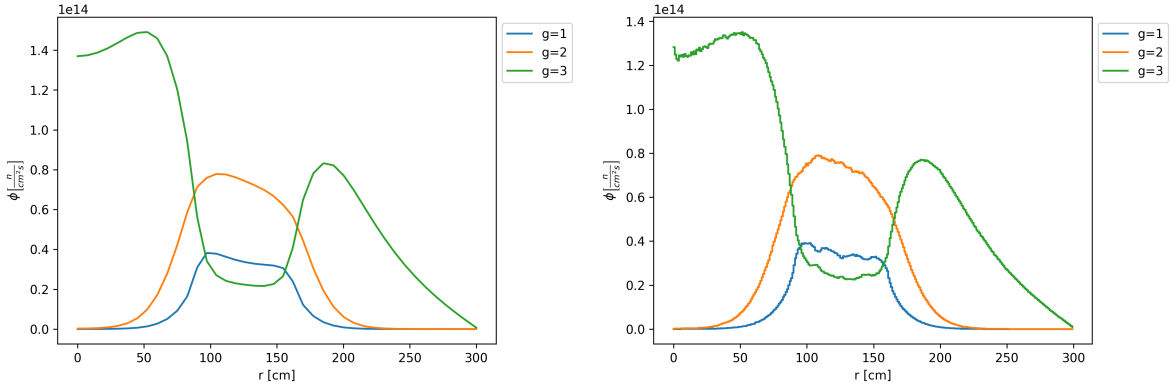

(a) Moltres. (b) Serpent.

Figure 6: Radial flux at 600 K.

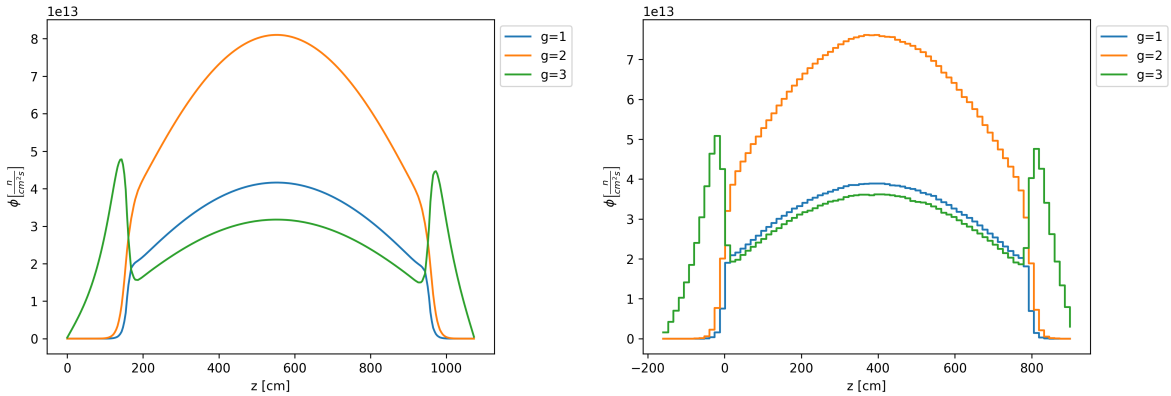

(a) (b) Serpent model geometry.

Figure 7: Axial flux at 1200 K.

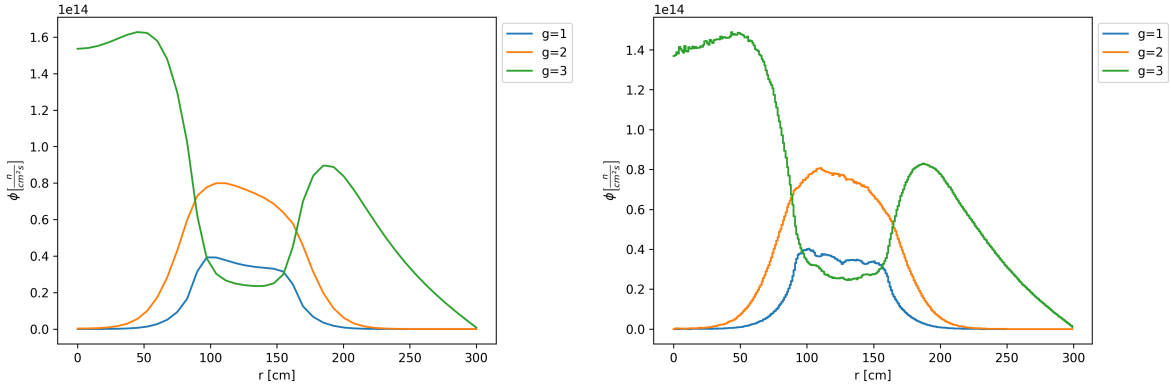

(a) Moltres.

(b) Serpent.

Figure 8: Radial flux at 1200 K.

1 OECD/NEA MHTGR-350 MW Benchmark: Phase I Exercise 1

This section conducted Phase I Exercise 1 of the benchmark with Moltres and compared the results with the already published results [1]. The benchmark specifies the cross-sections required to conduct the exercise. This ensures a common dataset among various benchmark participants. The files *OECD-MHTGR350_Simplified.xs xsmap.pdf* specify the group constants and the a detailed map of the constants numbering. The benchmark definition used DRAGON-4 [**?**] from a full block configuration. The dataset contains 26 energy groups. The exercise requests the reporting of the global parameters: K_{eff}, control rod (CR) worth ($\Delta\rho_{CR}$), and axial offset (AO). It also requires the reporting of the power distribution and a neutron-flux map [**?**]. Equations 1 and 4 define $\Delta\rho_{CR}$ and AO.

$$\Delta\rho_{CR} = \frac{k_{out} - k_{in}}{k_{out} k_{in}} \tag{1}$$

where

$$k_{out} = \text{eigenvalue with CR at position 1184.8 cm} \tag{2}$$
$$k_{in} = \text{eigenvalue with CR at position 391.81 cm} \tag{3}$$

and

$$AO = (TP_{top} - TP_{bottom})/(TP_{top} + TP_{bottom}) \tag{4}$$

where

$$TP_{top} = \text{total power produced in the top half core} \tag{5}$$
$$TP_{bottom} = \text{total power produced in the bottom half core.} \tag{6}$$

Figure 9 displays the geometry of the MHTGR-350. The model included a one-third of the reactor. The model considered the bottom and top reflectors. The fuel consisted of 220 assemblies. The simulations required two meshes. One for the control rod out (equation 1) and one for the control rod in. The simulation with the control rod out had 268393 DoFs/energy-group, and a total of 6978218 DoFs. The simulation with the control rod in had 227592 DoFs/energy-group, and a total of 5917392 DoFs. The Moltres input files set an eigenvalue convergence tolerance of 1×10^{-8}.

The benchmark exercise sets periodic boundary conditions on the the sides of the geometry. However, a memory issue did not allow for the implementation of those boundary conditions in our 26-group Moltres input file. We approximated the periodic boundary condition with the reflective boundary condition. Section 1.1 discuss further on the use of periodic and reflective boundary conditions.

On average, the simulations took 4.22 hours using 1024 cores. Table 2 shows the main results. Moltres predicted a K_{eff} larger than the reference result. The reactivity difference is of 99 pcm. Moltres yields a smaller control rod worth. The difference is of 312 pcm. The axial offset for the Moltres simulation is a 4% higher than the reference result. We attribute the discrepancies to the use of the reflective boundary conditions instead of the periodic boundary conditions. Once again, section 1.1 discuss further on the use of periodic and reflective boundary conditions.

Figure 10 shows the radially averaged axial power distribution. Moltres results look close in shape and magnitude to the reference results. Figure 11 shows the axially averaged radial power distribution. Moltres results are close to the reference results. Moltres power distribution in the inner ring is larger. The differences are within 0.25 W/cm^3.

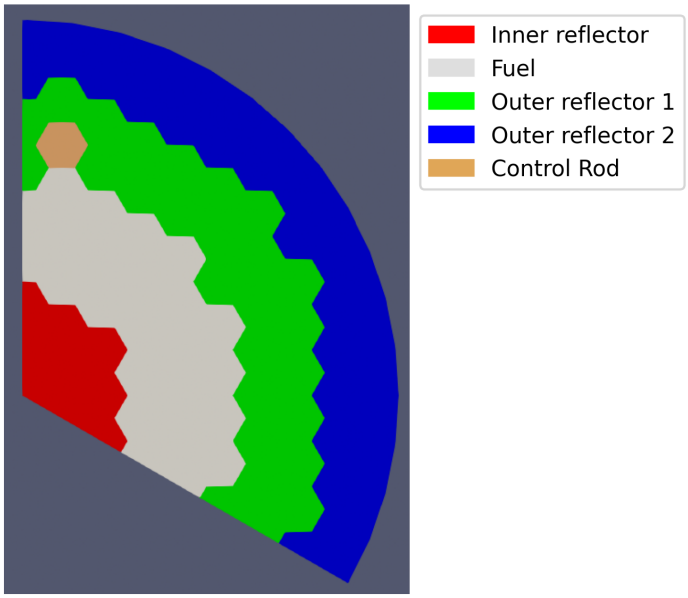

Figure 9: $1/3^{rd}$ of the MHTGR-350 geometry.

Table 2: Global parameters.

Parameter	Benchmark	Moltres
K_{eff}	1.06691	1.06804
$\Delta\rho_{CR}$ [pcm]	822.1	509.8
AO	0.168	0.1753

1.1 Periodic vs Neumann BCs

In the last section, we observed deviations in Moltres results. In this section, we analyzed the discrepancies that the reflective boundary condition approximation may introduce. As the last section mentioned, the memory requirements of the simulation limit the use of the periodic boundary conditions. To reduce the memory

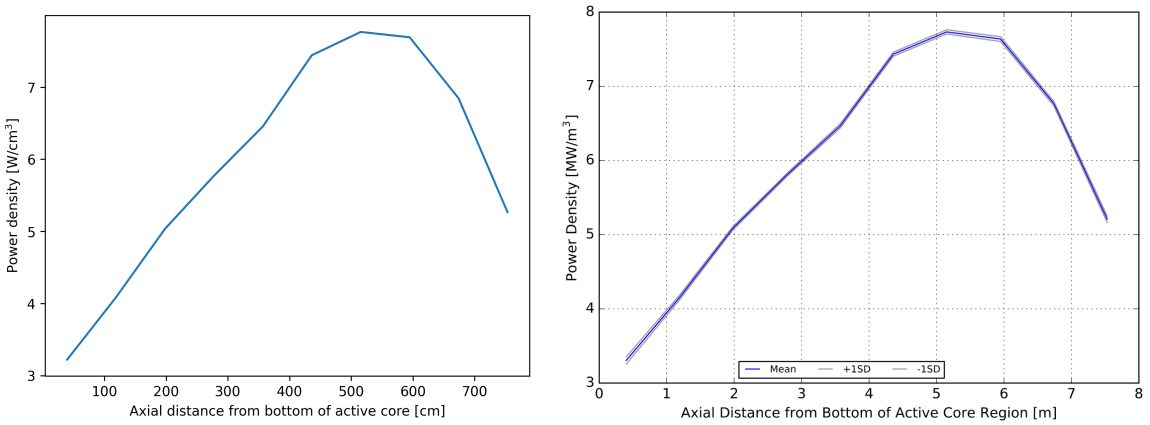

(a) Moltres result.

(b) Benchmark result. Image reproduced from [1].

Figure 10: Radially averaged axial power distribution.

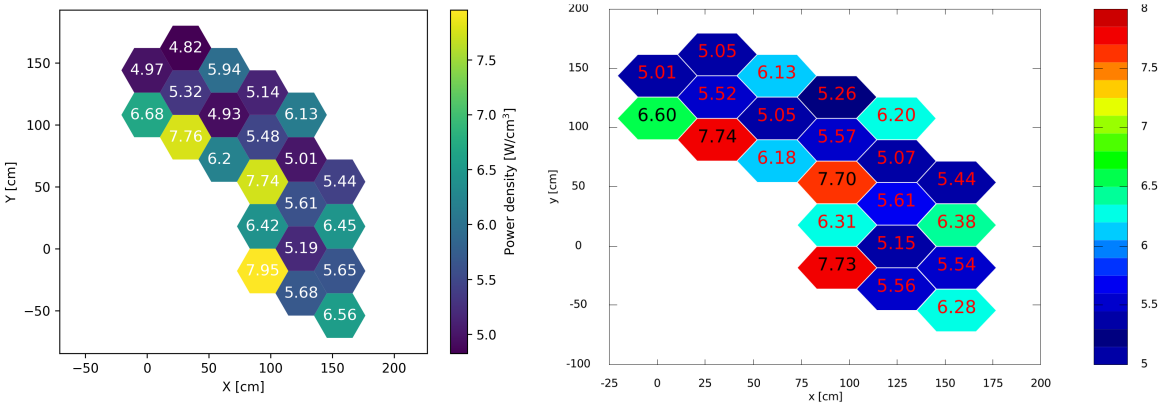

(a) Moltres result.

(b) Benchmark result. Image reproduced from [1].

Figure 11: Axially averaged radial power distribution.

requirements, we collapsed the group constants to a smaller number of energy groups. We simulated two cases: one that uses a 3-group structure and one that uses a 6-group structure. The simulations required two meshes each.

The 3-group simulation had 62118 DoFs/energy-group (total of 186354 DoFs) and 61596 DoFs/energy-group (total of 184788 DoFs) for the control rod out and control rod in cases, respectively. The 6-group simulation had 16898 DoFs/energy-group (total of 101388 DoFs) and 19116 DoFs/energy-group (total of 114696 DoFs) for the control rod out and control rod in cases, respectively. We highlight that the 6-group simulation had to use a coarser mesh, otherwise it would not run. This confirms the suspicion that the simulation's memory requirements prevents it from running.

For both cases, we ran simulations with periodic and neumann boundary conditions and we compared their results. Table 3 presents the results. The neumann boundary condition increases the K_{eff}. For the control rod out case, the increase is small. However, for the control rod in case, the increase is considerable. The combined effect of both increases leads to a decrease in the control rod worth. The axial offset results almost unaffected by the boundary condition approximation.

Table 3: Global parameters comparison for different types of BCs.

Energy groups	Type of BCs	$K_{eff,out}$	$K_{eff,in}$	$\Delta\rho_{CR}$ [pcm]	AO
3	Periodic	1.07571	1.06776	692.6	0.237
	Neumann	1.07586	1.07021	490.5	0.237
6	Periodic	1.07182	1.06356	724.3	0.185
	Neumann	1.07197	1.06610	513.3	0.186

2 Conclusions

The preliminary studies focused on several aspects of the simulations. The first aspect was the effect of distributing homogeneously the fuel compact isotopes in the Serpent model. The heterogeneous calculation took 28% more time. The results showed that the multiplication factor decreases considerably. Additionally, the homogenization of the fuel compact appears not to have a strong impact over the group constants. However, the considerable difference in the multiplication factor suggests that the combined effect of small variations in the group constants is significant. Although the particles' explicit modeling is time-consuming, it results necessary.

Focusing on a fuel column of the MHTGR-350, we investigated the effects of the energy group structure on the diffusion calculations. We considered four different operational cases: a fuel column without LBPs and a fuel column with LBPs, both cases at 600K and 1200K. Serpent obtained the homogenized group constants of the fuel column. Moltres took such constants as input with a Gmsh mesh. The first study compared the Moltres axial flux to Serpent axial flux. Moltres used a 26 energy group structure to run the simulations. Overall, the axial fluxes were close in shape and magnitude. A different study focused on the effects of the energy group structure on the K_{eff}. We note that the number of energy groups does not affect the accuracy of the eigenvalue calculations in Moltres. We also compared the L_2-norm relative error of the axial flux in the active core using different energy group structures. For the four operational cases, the accuracy improves increasing the number of energy groups. Additionally, we presented the simulation computational expense for the different number of energy groups. The simulation time and memory requirement rises increasing the number of energy groups. We notice as well that the computational time increases for the fuel column with LBPs. Finally, we analyzed the impact of using different 15-group structures on the L_2-norm relative error of the axial flux. We chose the $15d$ structure as the best performing.

References

[1] OECD NEA. Coupled Neutronic/Thermal- Fluid Benchmark of the MHTGR-350 MW Core Design: Results for Phase I Exercise 1, February 2020.